Ultrafast processes in Ag and Au: A Monte Carlo study

P. J. van Hall*
Department of Physics, Eindhoven University of Technology, P.O. Box 513, 5600 MB Eindhoven, The Netherlands
(Received 19 April 2000; published 15 February 2001)

Monte Carlo simulations of ultrafast electron processes in Ag and Au have been used to analyze transient reflectivity as well as two-photon photoemission experiments. The model consisted of an electron Fermi gas coupled to longitudinal acoustic phonons. A laser pulse of finite width excited the electrons, after which the development of the distribution function was followed during 3–5 ps. In the electron-phonon coupling we used the full q dependence of the scattering together with a semirealistic phonon dispersion relation. The strength of the electron-phonon scattering is governed by the deformation potential. Its value was fixed to low-fluence transient reflection data. Also hot-phonon effects were included. For the electron-electron scattering we employed a Coulomb interaction screened according to the Thomas-Fermi prescription. We accounted for exchange effects in the total scattering probability. In a later stage we varied the screening. We analyzed a variety of data for Ag and Au. A good description of the temperature dependence of the transient reflectivity for various excitation powers could be obtained. Also the time evolution of the Fermi surface showed fair agreement with the experiment. In the case of Ag the lifetime of an electron above the Fermi sea was predicted correctly. For Au, however, it was necessary to increase the screening to obtain the correct lifetimes of electrons excited above the Fermi sea. Using this adjusted screening the description of the other experiments no longer was appropriate. Finally also the resistivity due to electron-phonon scattering was predicted quite well using the deformation potential extracted from the ultrafast reflectivity experiments.

DOI: 10.1103/PhysRevB.63.104301 PACS number(s): 63.20.Kr, 78.47.+p

I. INTRODUCTION

The study of nonequilibrium processes in solid-state physics enables one to obtain information on dynamical aspects not accessible otherwise. For example, in semiconductor physics the study of the cooling of photoexcited carriers or of the carrier capture into quantum wells has delivered valuable information and new physical insights. The rich history can be found in the proceedings of the conferences on hot carriers.[1] The analysis and interpretation of the experimental results greatly benefitted from the technique of Monte Carlo simulation,[2] where one studies the time development of a cloud of representative particles. This method has found a widespread application in this field and has been developed to a high degree of sophistication.[3,4]

The investigation of similar phenomena in metals had to wait for the advent of ultrafast femtosecond lasers because of the much smaller times involved. While in semiconductors the cooling of excited carriers proceeds on a picosecond scale, in metals the time scale is well below the picosecond. Notably the carrier-carrier scattering is considerably faster due to the much larger number of electrons present. But by now ultrafast experiments have become a flourishing and rapidly expanding area of research. At present good experimental results on transient reflectivity on both thin[5–7] and thick films[8–10] of noble metals are available. Also, the development of the Fermi surface after laser excitation[11,12] and the lifetime of an electron above the Fermi sea[13–18] have been measured by two-photon photoemission experiments. Not only films of noble metals but also films of magnetic materials have been used in these types of experiments.[19–22]

Most of the earlier experiments have been analyzed in the two-temperature ($2T$) model.[23] Here one assumes that the electron and phonon systems are both in internal equilibrium but at different temperatures. This method has the virtue of accounting for the changes in the phonon system during the relaxation of the electron gas. The assumption of a permanent internal equilibrium, however, is very stringent and requires an infinitely fast electron-electron and phonon-phonon scattering. By now it has been well established that this approach fails for times below 1 ps, whereas the energy relaxation times also are in the order of 1 ps or less.

A second method is solving the Boltzmann equation more explicitly. Various attempts have been reported on in the literature. Groeneveld, Sprik, and Lagendijk[24] have solved the Boltmann equation but with the simplifying assumptions of both isotropic electron-electron and electron-phonon scattering. Sun *et al.*[7] used a realistic electron-electron interaction but treated the electron-phonon scattering in a relaxation-time approximation. These authors also accounted for the presence of the d band 2 eV below the Fermi level in Au. Bejan and Raseev[25] investigated the thermalization of the electron gas but in the absence of electron-phonon coupling. It is clear that magnetic systems present an even greater challenge. Up until now a transient MOKE experiment[19] has been analyzed in terms of a three-temperature model, where in addition a ''spin temperature'' has been introduced. Very recently Knorren *et al.*[26] calculated the electron lifetimes for nonmagnetic (Cu) as well as ferromagnetic (Fe, Co, and Ni) materials using realistic density of states. Only the electron-electron scattering was accounted for while assuming a scattering probability independent of the energy transfer. The authors also assumed the scattering for parallel and antiparallel electron spins to be the same. As we will show further on, this assumption is highly questionable.

To our knowledge no attempt has been made to apply the technique of the Monte Carlo simulation to this field, though it has proved its value in semiconductor physics. This ap-

proach has the advantage that it tries to describe all experimental data using the same microscopic interactions. However, a considerable coding effort is involved and one also needs good computing facilities. On the other hand, the alternative methods often introduce an effective coupling strength, which from the microscopic point of view is a complicated integral over interactions and the distribution function. Different observables have their ''own'' parameter and it is difficult to relate these numbers with each other. In an analysis using Monte Carlo simulations inconsistencies in parameters, etc., appear, directly pointing to deficiencies in the underlying physical model.

The aim of this paper can be seen as twofold. First we present an analysis to selected examples, viz., the temperature-dependent reflectivity data of Groeneveld, Sprik, and Lagendijk[5] on Ag and Au and of Juhasz *et al.*[6] on Au, the two-photon photoemission results of Fann *et al.*[12] on Au, and finally the lifetime measurements on Ag by Wolff and Aesclimann[17] and on Au by Cao *et al.*[18] All these experiments have been performed with very thin films, so we can assume a homogeneous heating. At the same time we gain insight about the applicability of the Monte Carlo method as a tool for the analysis of ultrafast experiments in metals.

The organization of this paper is as follows. In the next section we expose the theory and the other ingredients that are part of our simulations. We then present the results of an example and discuss them extensively to see to see what we can learn. Section IV is the main part of this paper. Here we analyze a number of experimental results. Finally we draw some conclusions about the models involved and about the applicability of the Monte Carlo simulations in this field of ultrafast processes in metals.

II. THEORY AND MODELING

In the ultrafast laser experiments one generates hot electrons above the Fermi level. These electrons rapidly distribute their energy by electron-electron collisions. The hot gas subsequently cools down by transferring its energy to the phonon system. Roughly speaking this cooling process will depend on the number of electrons excited above the Fermi sea, because only these are able to lose their energy by creating phonons. In the very first stages of the relaxation we expect this number to increase due to electron-electron scattering, leading to an increase in the energy-loss rate and thus (strong) nonlinear effects in the cooling process. So we have an interplay between electron-electron and electron-phonon scattering. It is worthwhile to point out here that one of the basic assumptions of the $2T$ model is that the electron thermalization process is infinitely fast. We therefore have to specify the electron-phonon and the electron-electron interaction. Before doing so we briefly discuss the band structure used in our simulations.

A. Band structure

All noble metals have a fcc crystal structure. We use a simple spherical Brillouin zone as a model. We also assume that the electrons can be described as a free-fermion gas with a spherical Fermi surface, though we know that the real Fermi surface has a neck at the L point.[27] Another simplification is the neglect of the d band. This might be justified better in Ag, where the d band is 4 eV below the Fermi level, than in Au, where this distance is only 2 eV.[27] Actually the same approximations have been made, although implicitly, in the $2T$ model and in some of the solutions of the Boltmann equation.

B. Electron-phonon scattering

The electron-phonon coupling proceeds via deformation potential scattering by longitudinal acoustic phonons.[4,28] In contrast with semiconductors, we should not include screening explicitly, since the deformed crystal potential already contains these effects via the Born-Oppenheimer approximation. The matrix element reads

$$V^{\pm}_{e\text{-ph}}(q) = V_D q[(\hbar/2\rho\omega_q)\{N_q + \tfrac{1}{2} \pm \tfrac{1}{2}\}]^{1/2}, \tag{1}$$

where the plus and minus sign refer to emission and absorption, respectively, and N_q stands for the phonon occupation number, which in thermal equilibrium is given by the Bose-Einstein distribution. In this expression ρ is the density and ω_q the phonon frequency. The strength is governed by the deformation potential V_D, which is an adjustable parameter.

The intrinsic q dependence in Eq. (1) together with the available phase space results in a phonon production peaking at large q. This feature makes the choice of the dispersion relation especially at the end of the Brillouin zone important. We used the following approximation:

$$E_q = \hbar\omega_q = E_0 \sin(\pi q/2Q_0). \tag{2}$$

Here Q_0 is the limit of the Brillouin zone. With the empirical value of the longitudinal sound velocity ($v_{\text{lo}} = \pi E_0/2\hbar Q_0$) the maximum energy E_0 is 10–20 % too high. Due to the peaking of $W_{e\text{-ph}}(q)$ at high q this may overestimate the energy relaxation. We therefore used in Eq. (2) the empirical energy at the edge of the Brillouin zone.[29] The combined effect of Eqs. (1) and (2) results in the production of nearly monoenergetic phonons with energy E_0.

As the momentum transfers are rather high, umklapp scattering can occur. However, the combination of the momentum **k**, the momentum transfer **q**, and the reciprocal-lattice vector **G** is such that energy is conserved. Analogous to Bragg reflection this restriction gives only a few allowed points in phase space. We therefore neglected these processes. Moreover, the possible small contribution is accounted for in the fitted value of V_D.

Due to the phonon creation the phonon occupation N_q changes with time and thus does the electron-phonon scattering. In our calculations we accounted for these ''hot-phonon'' effects[30] by frequently updating $V_{e\text{-ph}}(q)$. There are several arguments why it may be important to incorporate these effects even at low excitation densities. First, due to the Pauli principle the absorption of phonons is hindered much less than the emission. So even the presence of a small number of extra phonons may have a noticeable effect. Sec-

ond, the created phonons are at the edge of the Brillouin zone and have a low group velocity and do not escape from the interaction volume. This implies that we are dealing with an accumulating phonon distribution. There is clear experimental evidence that these effects are important. Even in the experiments with very low intensity by Groeneveld, Sprik, and Lagendijk[5] the transient reflection did not return to its initial value.

In our calculations we did not account for phonon-phonon interactions. This means that we allowed the accumulated phonon distribution to be far from equilibrium. An alternative would have been to thermalize the phonon distribution permanently as is done in the $2T$ model. With respect to the $2T$ model the coupling to longitudinal phonons only has implications for the specific heat entering the rate equations. In the absence of phonon-phonon interaction the specific heat should be C_v for the longitudinal phonons only viz., about $\frac{1}{3}$ of the normal total C_v due to the lattice. If there is energy transfer to the transversal branches one has to complement the equations with a third one describing this transfer.

C. Electron-electron scattering

For the electron-electron interaction we used a screened Coulomb potential. The matrix element between plane waves reads

$$V_{e\text{-}e}(q)=e^2/\epsilon_0\epsilon_r(q^2+\lambda^2), \tag{3}$$

where q is the transferred momentum. There is some uncertainty about the value of the screening parameter λ. For the present we adopt for λ the inverse Thomas-Fermi screening length λ_{TF} given by[28]

$$\lambda_{\mathrm{TF}}^2=e^2m^*k_F/\pi^2\epsilon_0\epsilon_r. \tag{4}$$

Here k_F is the Fermi momentum. Of course this static screening is a crude approximation to the real situation. Especially on very short time scales one would like to use dynamical screening. One of the aims of this paper is to investigate the limits of the static approach.

A few remarks, however, already can be made. As k_F is nearly temperature independent due to the high electron concentration, the same holds for λ_{TF}. So the exact shape of the distribution function is not very important. This, however, may not be the case when the number of particles changes by excitations from the d band. We therefore expect this approximation to be better in the case of Ag than in the case of Au. Indeed as will be shown later when discussing the lifetime experiments we need additional screening for Au, probably due to rearrangements of the holes inside the d band. Therefore at the end of this paper we shall treat λ as an adjustable parameter.

In electron-electron scattering one has to discern between scattering with parallel spins and scattering with antiparallel spins. In scattering with parallel spins terms due to antisymmetrization arise. Usually they are omitted because of the difficulties involved.[31] We have investigated their contribution using the formalism described elsewhere.[32] We calculated separately the scattering probability for parallel and antiparallel spins. The results are given in Fig. 1. The scattering

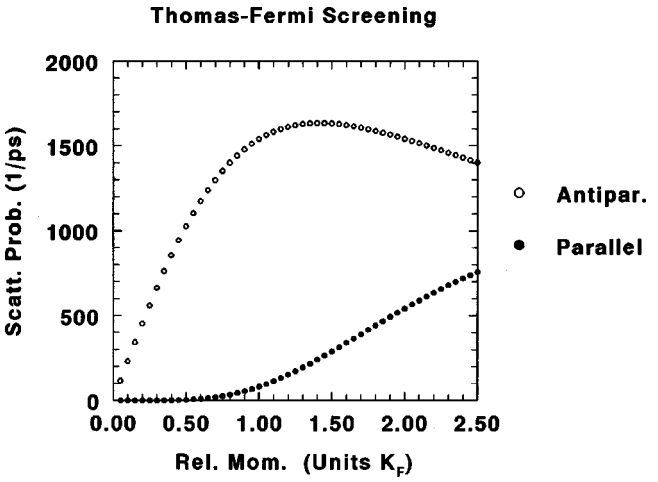

FIG. 1. Comparison between electron scattering with spins parallel and with spins antiparallel for the case of Ag as dependent on the relative momentum. A screened Coulomb potential (Thomas-Fermi screening) has been used as the *e-e* interaction.

between particles with parallel spins is strongly suppressed due to the negative interference between the direct term and the exchange term. We find a ratio of 6 between the average scattering with antiparallel spins and with parallel spins. It is clear that the assumption of spin-independent scattering[26] is highly incorrect. One can neglect the parallel spin scattering better.

It is very difficult to incorporate the correct angular dependence of the scattering of particles with parallel spins into a Monte Carlo simulation. We therefore adopted the following hybrid procedure. The total scattering cross section has been calculated with inclusion of the exchange terms in order to obtain the correct total scattering rates. For the differential cross section, however, we used Eq. (3), viz., we neglected

TABLE I. Parameters.

	Ag	Au	Units
Number carriers	5.86	5.89	$10^{23}\,\mathrm{cm}^{-3}$
Fermi energy E_F	5.50	5.52	eV
Fermi momentum k_F	12 016	12 036	$\mu\mathrm{m}^{-1}$
Thomas-Fermi screening λ_{TF}	17 015	17 030	$\mu\mathrm{m}^{-1}$
Lattice constant a	4.09	4.08	Å
Brillouin zone O_0	15 362	15 400	$\mu\mathrm{m}^{-1}$
Density ρ	10.40	19.32	$\mathrm{g/cm}^3$
Max. phonon energy E_0	19.96	19.07	meV
V_{sound}[a] (longitudinal)	3650 (3100)	3240 (2955)	m/s
Deformation potential V_D[b]	3.7 (0.1)	4.6 (0.1)	eV
Resistivity[c] (300 K)	1.62 (1.65)	2.24 (1.53)	$\mu\Omega$/cm
Adjusted V_D		5.8 (0.1)	eV
Adjusted screening $\lambda/\lambda_{\mathrm{TF}}$		1.50	
Exponent γ in fit V_D	2.12	2.26	

[a]The number in parentheses is the value deduced from the maximum phonon energy E_0.

[b]The number in parentheses is the estimated error.

[c]The number in parentheses is the theoretical value.

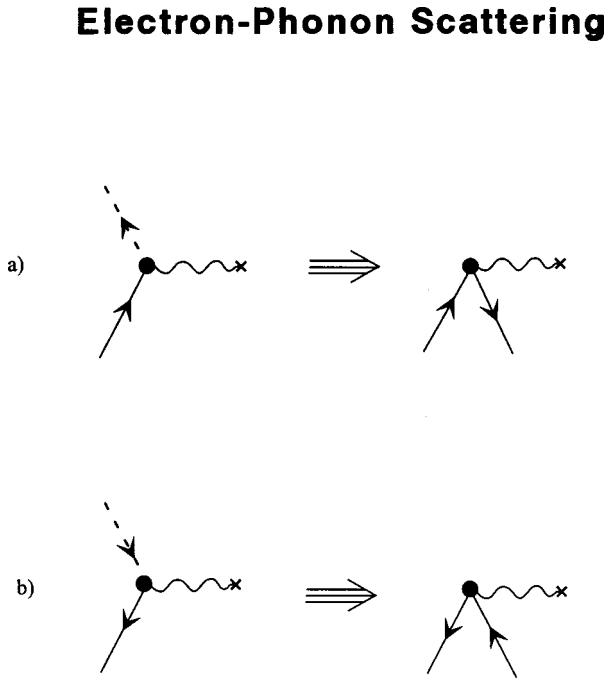

FIG. 2. Feynman diagrams for (a) the emission of a phonon by an electron, in which the final state is below the Fermi level (dashed line) and (b) the emission of a phonon by a hole, in which the final state is above the Fermi level (dashed line). Applying time symmetry gives the same diagram, viz., the recombination of an electron and a hole with the emission of a phonon.

the change in shape due to exchange terms. This approximation is not a serious one. The value of λ_{TF} (see Table I) is larger than the Fermi momentum k_{F}. This gives a rather weak dependence of the scattering on the angle.

The electron-electron scattering rate is often parametrized as follows. According to Pines and Nozières[33] the lifetime of a quasiparticle with energy E above the Fermi sea ($E>E_F$) is given by

$$\tau=\tau_0\{E_F/(E-E_F)\}^2, \tag{5a}$$

$$\tau_0=128/\sqrt{3}\,\pi^2\omega_p\,, \tag{5b}$$

$$\omega_p^2=ne^2/\epsilon_{0_m} \quad \text{(the plasmon frequency)}. \tag{5c}$$

In this expression the scaling factor τ_0 is given by the Fermi liquid theory (FLT) under the assumption that the mean distance between the electrons is small compared to the Bohr radius.[34] These conditions are not met in Ag and Au, where the ratio is about 3. The value of τ_0 following from Eq. 5(b) is 0.55 ps. It also can be determined empirically by means of Monte Carlo simulations, where one records the evolution of the number of electrons in a small interval around E (see also the discussion of the lifetime experiments in Sec. IV). We found the dependence of τ on E as given by Eq. 5(a) but with a value for the scaling factor τ_0 of 1.04 fs.

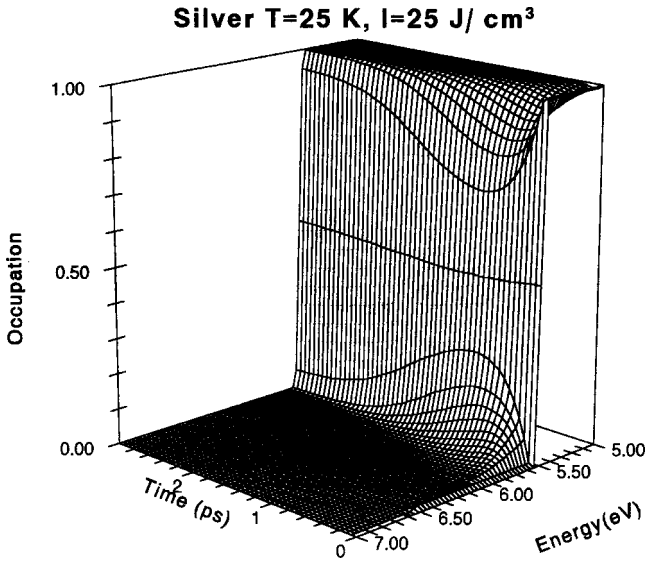

FIG. 3. Three-dimensional plot of the time development of the distribution function for Ag after excitation with a δ laser pulse. The laser energy E_x is 1 eV, the temperature T is 25 K, and the dissipated power I is 25 J/cm^3.

D. Particle-hole representation

An important obstacle in the feasibility of the Monte Carlo method for simulation of ultrafast processes in metals is the large number of carriers in the conduction band. Compared with semiconductors this number is at least 4 orders of magnitude larger. This would imply that also the number of particles used in the simulation had to be larger by the same factor. Moreover, the collisions of particles deep inside the Fermi sphere are Pauli forbidden, making the simulation in addition very inefficient. We generally circumvented this problem as follows.

First, we assumed that electrons deeper in the Fermi sea than the laser energy E_x are not involved in the relaxation processes as nearly all their collisions are Pauli forbidden. So we could restrict our model space to the outer part of the Fermi sphere (viz., $E_{\mathrm{el}}>E_F-E_x$).

Second, we have chosen a different representation of the system. Besides the standard formulation with electrons, one also can characterize the distribution function in terms of electrons above and holes below the Fermi energy at $T=0$ K. Especially at low temperatures this results in a tremendous reduction of particles participating in the simulation. However, the program becomes more complicated. In addition to the electrons, the holes interact with phonons and each other. Moreover, we have to allow for the creation and annihilation of electron-hole pairs, so the number of particles is not constant with time. Nevertheless, we gained a factor of 5–25 in efficiency, depending on the temperature and excitation density. Moreover, since we simulate the disturbances of the distribution function and not the distribution as a whole, we also gain in accuracy.

However, one has to be careful to avoid double counting. As an example, an electron emits a phonon and is scattered below the Fermi level. When the collision is not Pauli forbidden there is a hole at that energy and so pair annihilation

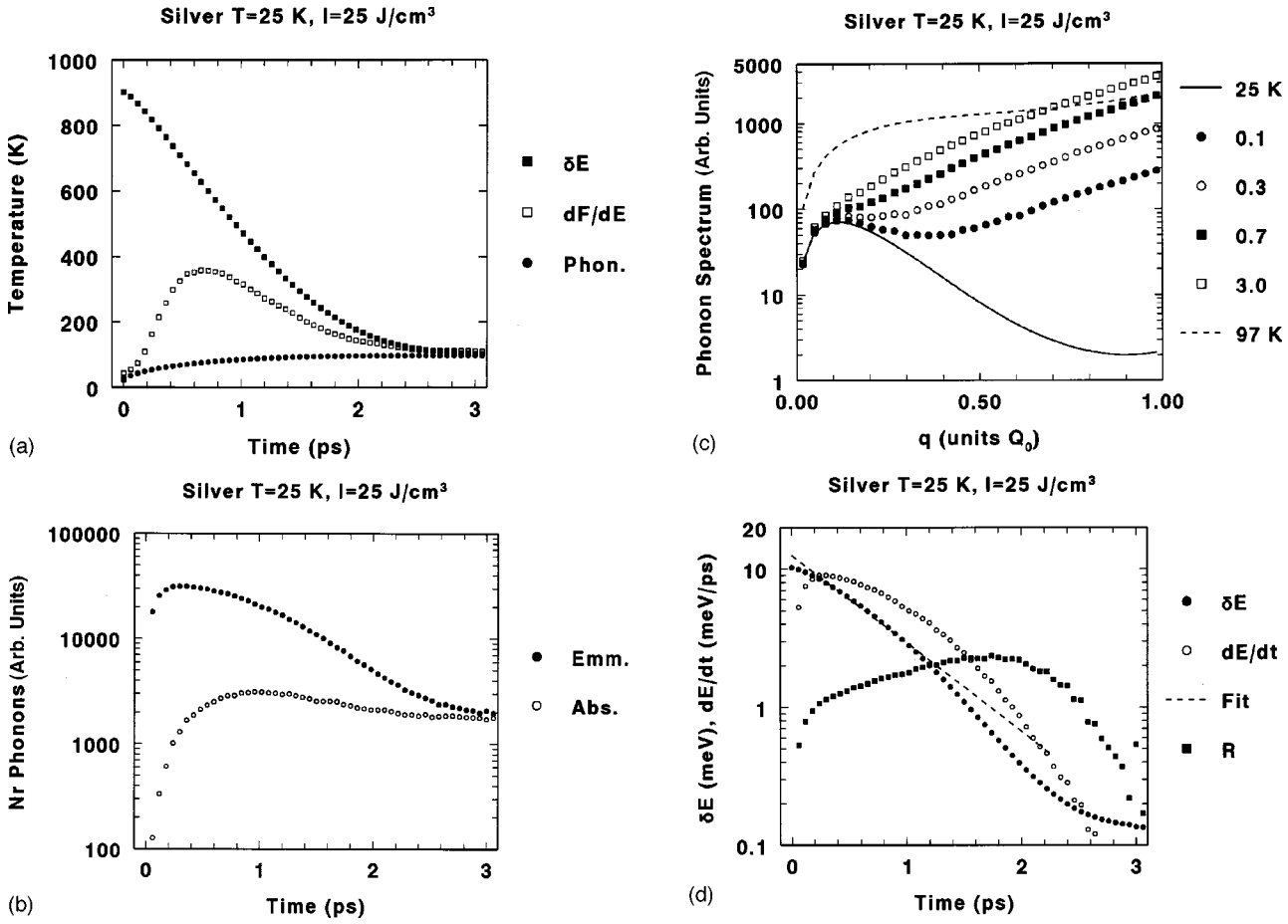

FIG. 4. (a) Time development of phonon and electron temperatures. For the definitions of the temperatures see text. (b) Phonon emission and absorption rates. (c) The time dependence of the phonon spectrum. (d) The excess energy δE and and energy-loss rate dE/dt, R is the ratio between dE/dt and δE.

occurs. Similarly a hole can emit a phonon and end above the Fermi level. If we draw the corresponding diagrams as shown in Figs. 2(a) and 2(b), we see that these processes are equivalent—the recombination of a hole and an electron with the emission of a phonon. In order to avoid double counting we have to skip one of the channels. Similar diagrams occur in electron-electron scattering. This happens whenever we deal with the annihilation of a pair, since we can start with either an electron or with a hole.

III. SIMULATIONS

The basic result of our simulations consisted of time-dependent distribution functions. From these distribution functions we derived various quantities. First, we calculated the difference in energy $\delta E(t)$ as compared with the energy E_0 of a Fermi-Dirac distribution at $T=0$ K. The relaxation time of this excess energy is the same as the relaxation time seen in the transient reflection experiments.[35,36] However, a warning should be given. This equivalency has been derived under the assumption of a thermalized distribution. As stated before, in the first few hundreds of femtoseconds after the laser excitation this certainly is not the case.

Nonlinear effects can be better seen in the derivative—the energy-loss rate—so we also recorded this quantity. In addition we calculated the slope of the distribution function around the Fermi level and thus found the temperature T_{el}^1 of the electron gas. A way to define the electron temperature T_{el}^2 is to look at the total energy content of the electron gas, as is done in the $2T$ model. Only if the distribution is thermalized completely do these two temperatures coincide. Analogously we can assign a temperature T_{ph} to the phonon system based on the total energy, though the phonons are not in a thermal equilibrium. The parameters used in our simulations together with derived quantities can be found in Table I.

A. Example

We now want to illustrate the foregoing process with an example. We have chosen a low temperature and a relatively strong excitation with a δ pulse of 1 eV to emphasize the various features. In Fig. 3 we give the three-dimensional plot of the distribution function. The excitation of electrons from the Fermi sea at zero time is hardly visible, but the subsequent thermalization can be seen clearly. It should be noticed that this thermalization takes about 0.5 ps, clearly indicating the insufficiency of the $2T$ model. After 3 ps we end with an electron distribution, which is still quite hot (97 K) due to the

hot-phonon effects. This is illustrated more clearly in Fig. 4(a), where we plot the electron and phonon temperatures (due to the discretization the electron temperature T_{el}^{1} does not have the nominal value of 25 K at zero time). The two electron temperatures only coincide after 2 ps. The thermal equilibrium between phonons and electrons is reached after 2.5 ps at a temperature around 97 K. The numbers of created and absorbed phonons are now again the same, but at a level more than 2 orders of magnitude larger than at the original temperature [see Fig. 4(b)]. This is due to a large increase in N_q and accordingly in the e-ph scattering rates [Eq. (1)]. In Fig. 4(c) we show the phonon spectrum as a function of time together with the spectra for thermalized distributions at 25 and 97 K. The enhancement of scattering with large q as discussed previously is clear and results in a nonthermal distribution.

It should be noted that the energy-loss rate—in the beginning equivalent to the number of emitted phonons—still increases during the first 0.2 ps and decreases only slowly afterwards. In these circumstances one cannot expect an exponential relaxation of the electron excess energy $\delta E(t)$. This is clearly visible in Fig. 4(d), where we show δE together with the fit derived for the region between 0.3 and 1.5 ps. It also is instructive to plot the ratio R between the excess energy $\delta E(t)$ and the energy loss dE/dt. For a purely exponential decay this quantity should be time independent. In the same graph we see that R increases with time during the most relevant part of the energy relaxation, clearly indicating a faster than exponential decay during the first 1.5 ps as more and more electrons participate in the cooling process. In the first 400 fs the number of excited electrons increases by a factor of 3.

B. Analysis

The energy relaxation times were derived from the time dependence of $\delta E(t)$. After folding with the experimental resolution the curves were analyzed assuming

$$\delta E(t) = A \exp(-t/\tau) + B, \tag{6}$$

where the constant background B has been introduced to account for the zero-time energy and for hot-phonon effects.

There exist various sources of uncertainty in the extracted value of τ. To begin with—as we have seen—the decay is nonexponential. This means that the value of τ will depend on the interval used for the fit. We therefore varied the interval used in the fit between 0.2 and 1.2 ps and between 0.3 and 1.5 ps. From the variation in τ we deduced the uncertainty. Moreover, the fit is far from perfect, resulting in an additional error.

Furthermore, it should be noticed that although the results of the simulation are processed as if they were independent and uncorrelated experimental data, in fact they are highly correlated, because the value of $\delta E(t)$ emerges from the value at $t-\delta t$. This means that another random sequence may give a different value of τ. This intrinsic uncertainty is due to the statistical nature of the Monte Carlo procedure. We tried to estimate this uncertainty by performing four equivalent simulations and averaging the results. The total error of τ as given in the graphs is a combination of all these effects. Moreover a visual impression can be obtained from the scatter and smoothness of the theoretical results when we compare them with experimental data in the next section.

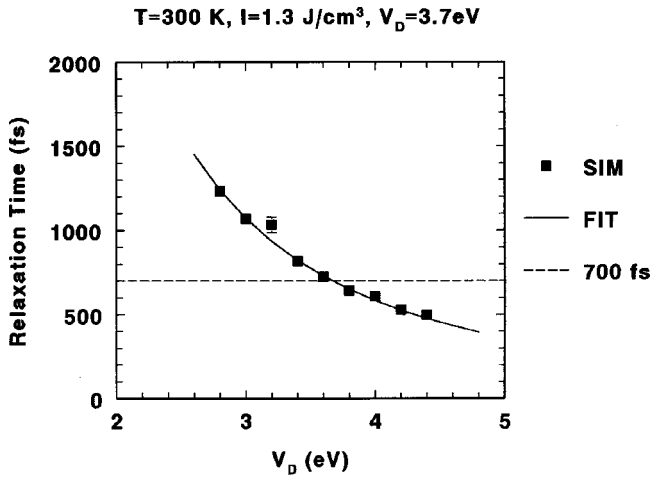

FIG. 5. Results of the search for V_D in the case of Ag. The assumed relaxation time is 700 fs. The solid curve is a fit with $\tau = 700(3.7/V_D)$.[2,12]

IV. RESULTS AND DISCUSSION

A. Search for V_D

The first step in our analysis is the search for V_D. For this we used the values of the relaxation time as obtained by Groeneveld, Sprik, and Lagendijk.[5] The excitation density was quite low (1.3 J/cm^3). We chose a temperature of 300 K, because we expect the effects of hot phonons here to be minimal. A series of calculations with different V_D has been performed. From Eq. (1) we expect a dependency of τ as $1/V_D^{\gamma}$, with the exponent γ around 2. So we fitted the results accordingly. As can be seen from the results in Table I, γ is only slightly higher. The uncertainty in V_D is about 0.1 eV, apart from the error due to the experimental uncertainty (about 5%). An example of the calculated relaxation times together with the fit is displayed in Fig. 5. These calculations have been done with statistics equivalent to 3×10^6 particles in the model space for a particle Monte Carlo simulation. Note that the theoretical results are averages over four equivalent calculations with a different random sequence.

B. Energy relaxation

The first experimental item we investigated is the temperature dependence of the energy relaxation time. In Figs. 6(a) and 6(b) we show the experimental data of Groeneveld, Sprik, and Lagendijk[5] together with our theoretical results. Here again we performed four equivalent simulations with 3×10^6 particles and averaged the results. The agreement between experiment and theory is quite good, though for Au the calculated low temperature results are a bit too high.

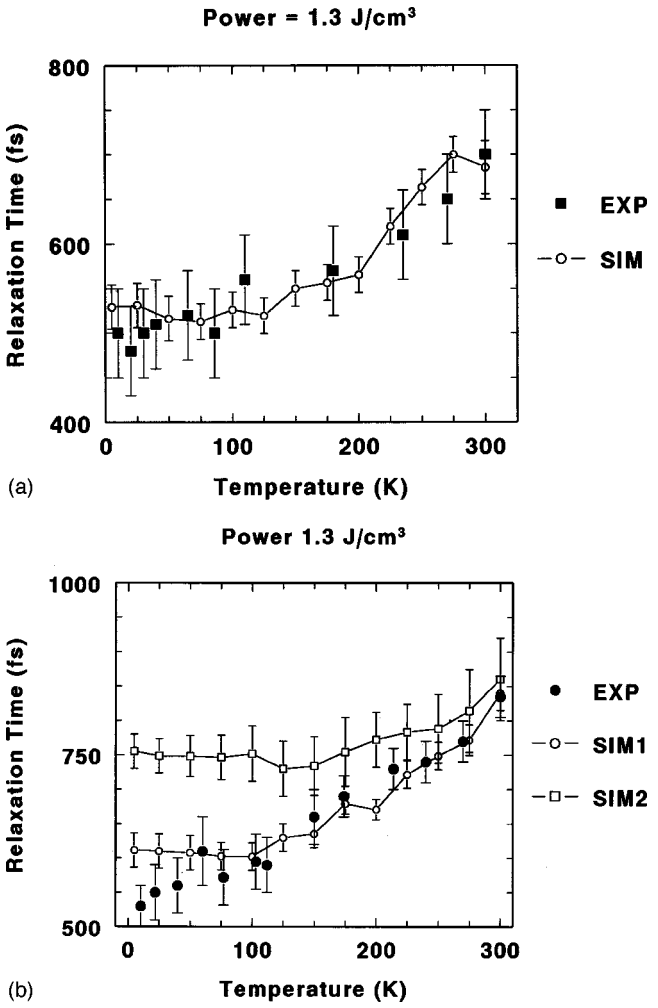

FIG. 6. (a) Comparison of experimental and calculated relaxation times. Experimental results of Groeneveld, Sprik, and Lagendijk (Ref. 5) for Ag. (b) As in (a) for Au. SIM1: $V_D = 4.6$ eV, $\lambda = \lambda_{TF}$; SIM2: $V_D = 5.8$ eV, $\lambda = 1.50\lambda_{TF}$.

Juhasz *et al.*[6] also have measured the energy relaxation time for Au but at a considerable higher laser fluence (20 J/cm^3). We expect a slower relaxation because of two reasons. First, the hot-phonon effects are much stronger here [see Figs. 3(b) and 3(c)]. In addition, we have seen that a higher temperature gives a slower relaxation [Figs. 6(a) and 6(b)]. A stronger excitation results after the first few hundreds of femtoseconds in a thermalized electron gas with a higher temperature and a corresponding slower relaxation. It is also clear that the temperature dependence will be weaker, when the excitation becomes stronger. All these features can be seen when we compare Fig. 6(b) with Fig. 7. Our calculations (denoted by SIM1) give an excellent description of the data, especially when one takes into account that these calculations did not involve any fitting of parameters.

First, one would like to attribute the temperature dependence to N_q. However, we deal with the net phonon emission, viz, $W^-(q) - W^+(q)$, which is temperature independent since the terms with N_q cancel [Eq. (1)]. When we turn off the electron-electron scattering the relaxation times are about one order of magnitude higher and largely independent

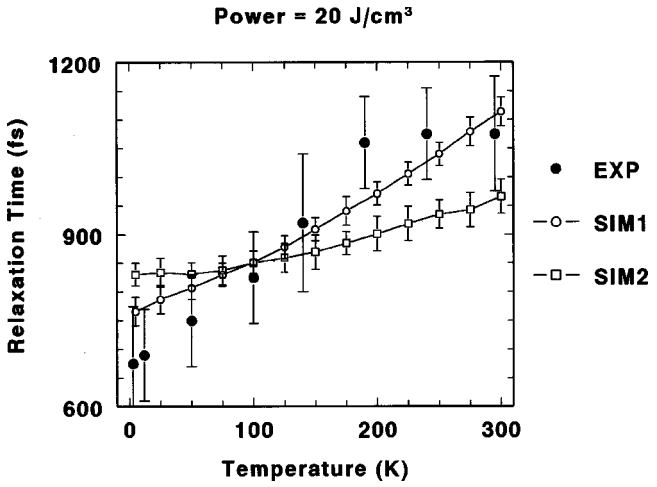

FIG. 7. Comparison of experimental and calculated relaxation times. SIM1: $V_D = 4.6$ eV, $\lambda = \lambda_{TF}$; SIM2: $V_D = 5.8$ eV, $\lambda = 1.50\lambda_{TF}$. Experimental results of Juhasz *et al.* (Ref. 6) for Au.

of temperature and incident power. So the electron thermalization of the electron distribution is responsible for the temperature and power dependence. This thermalization is slower if more electrons are above the Fermi level (high temperatures and high powers), which, due to the Pauli principle, hinder the excitation of cold electrons. As will be discussed below, we also performed calculations with a stronger screening. These calculations [indicated by SIM2 in Figs. 6(b) and 7]. This weaker interaction does not describe the temperature dependence of the relaxation time. The fact that our calculations describe the temperature and power dependence quite well justifies our choice of the electron-electron interaction, viz., the Thomas-Fermi screening.

C. Photoemission experiments: Electron temperature

A different type of experiment has been performed by Fann *et al.*[11,12] By a two-photon emission experiment these authors measured the time dependence of the distribution function in Au. In particular the slope around the Fermi level has been measured and parametrized in terms of a temperature analogous to our definition of $T_{\rm el}^1$. As has been shown above, the time development of $T_{\rm el}^1$ is very sensitive to the *e-e* scattering. In Figs. 8(a) and 8(b) we compare their experimental points with our theoretical results (indicated by SIM1). Unfortunately the experimental laser fluence had an uncertainty of 30%. We therefore also performed simulations at the upper and lower limits. It seems that at low excitation densities the theoretical thermalization is somewhat faster than the experimental one, resulting in higher peak temperatures. At higher laser power the theoretical values match the experimental ones well. This overall agreement between experiment and calculations, however, is quite satisfactory and also corroborates the applicability of our approach and of the parameters used (V_D and λ).

D. Photoemission experiments: Electron lifetimes

In a two-photon photoemission experiment one can also measure the lifetime of an electron far above the Fermi level.

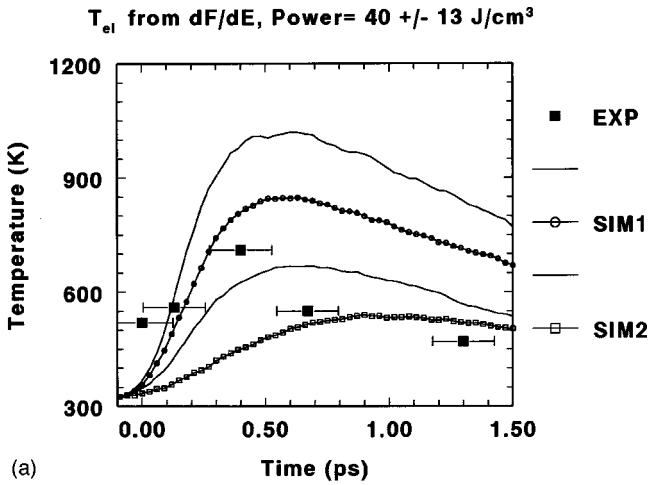

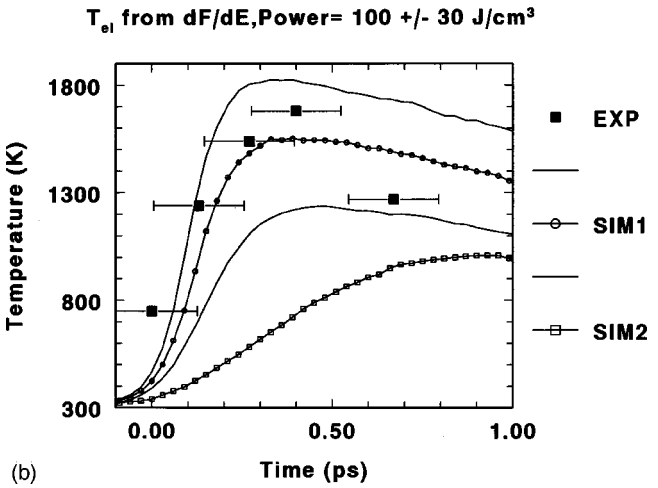

FIG. 8. (a) Experimental and calculated time development of the slope of the Fermi surface expressed as an effective temperature. SIM1: $V_D=4.6$ eV, $\lambda=\lambda_{TF}$; SIM2: $V_D=5.8$ eV, $\lambda=1.50\lambda_{TF}$. Experimental results of Fann *et al.* (Ref. 12). (b) As in (a) for a higher laser fluence.

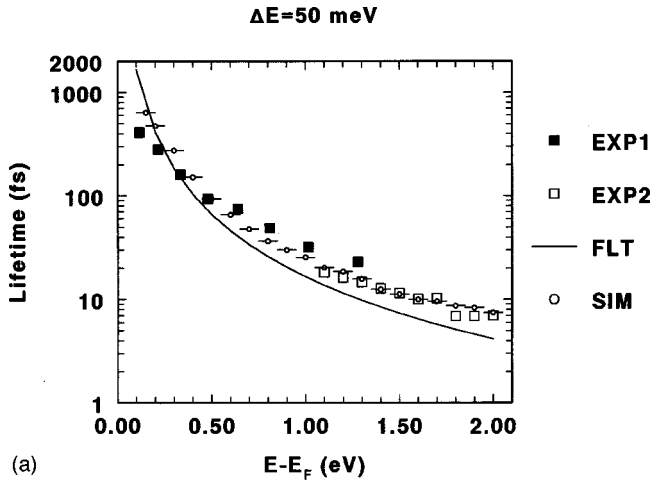

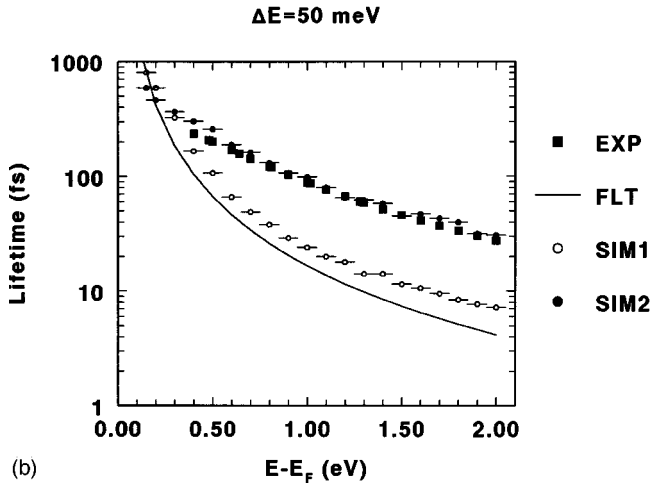

FIG. 9. (a) Experimental and calculated lifetimes of electrons in Ag. FLT: Results using the Fermi liquid theory [Eq. (5)]. SIM1: Results with *e*-ph and *e*-*e* scattering. SIM2: Results with *e*-*e* scattering only. Experimental results of Wolff and Aesclimann (Ref. 17). (b) Experimental and calculated lifetimes of electrons in Au. FLT: Results using the Fermi liquid theory [Eq. (5)]. SIM1: Results using $V_D=4.6$ eV and $\lambda=\lambda_{TF}$; SIM2: results using $V_D=5.8$ eV and $\lambda=1.50\lambda_{TF}$. Experimental Results of Cao *et al.* (Ref. 18) using the empirical relation given by the authors.

We analyzed the experiments of Wolff and Aesclimann[17] for Ag and of Cao *et al.*[18] for Au. In these analyses we varied the laser energy E_x and recorded the content of the energy bin at the upper end of the spectrum ($\Delta E=100$ meV). This is in contrast with experiment, where one uses a rather high laser energy (for example,[18] 3.2 eV) and measures all the lifetimes simultaneously. The energy bins with $E<E_x$, however, suffer from interscattering, and an elaborate analysis is necessary to extract the lifetimes. In all simulations we used a modest excitation density, viz., 10 J/cm^3.

We restricted our calculations to lifetimes for $E\leqslant 2.0$ eV for two reasons. First, at higher energies we come outside the range of validity of our model (viz., the neglect of the *d* band). Moreover, it is highly dubious if these classical Monte Carlo simulations are valid when the lifetimes are below 10 fs. The appropriate analysis is then solving the Bloch equations.[37]

The results for Ag have been depicted in Fig. 9(a) together with the results of Wolff and Aesclimann.[17] These consist of two series of data, which differ somewhat. It can be seen that the complete calculations describe the data quite well. At high energies the *e*-*e* scattering dominates, while at low energies the inclusion of *e*-ph scattering is necessary. When we compare the results[35] of the FLT [Eq. (5)] with those obtained without *e*-ph scattering, we see that the FLT predicts lifetimes roughly a factor 2 too low. As said before, this might be due to the assumptions used to derive Eq. (5).

We now compare experiment and theory for Au [see Fig. 9(b)]. However, in contrast to Ag the experimental and calculated values do not match at all. Roughly speaking there is a difference of about a factor of 4. A reason for this discrepancy can be the following. Our choice of the Thomas-Fermi screening length is somewhat arbitrary. If the electrons of the *d* band are involved, they certainly also contribute to the screening. These experiments on Au have been performed with a laser energy of 3.2 eV, so a substantial fraction of the excited electrons originates from the *d* band. This certainly will affect the results. We therefore increased the inverse

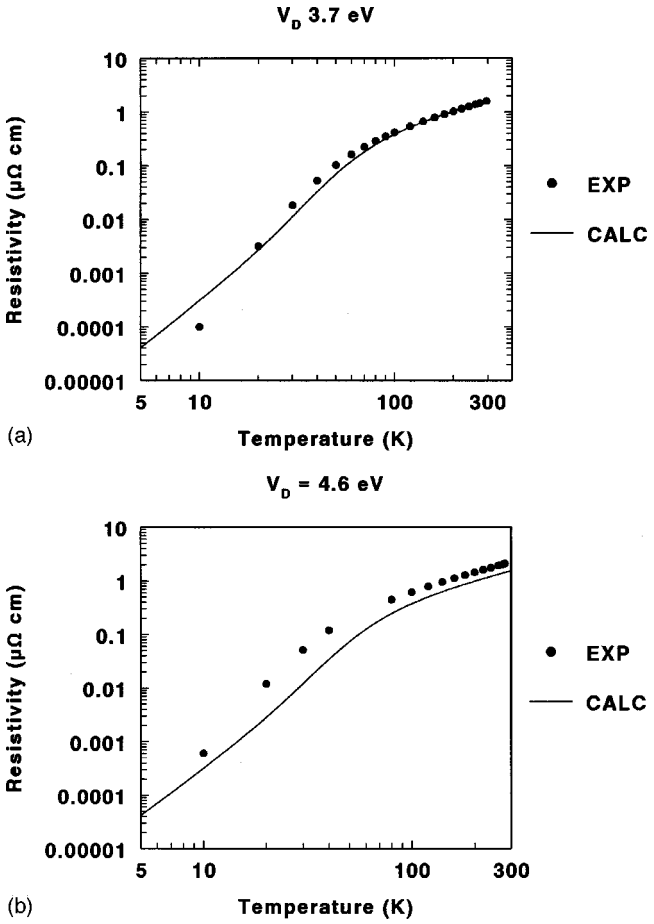

FIG. 10. (a) Comparison of experimental (Ref. 30) and calculated resistivity for Ag. (b) As in (a) for Au.

screening length with a factor 1.5 and repeated the calculations [SIM2 in Fig. 9(b)]. Now there is a very good agreement between experiment and calculations. As said earlier both *e*-ph and *e-e* scattering contributes to the energy relaxation, so we have to check the effect of the increased screening in the calculations of the energy relaxation and of the electron temperature.

E. Calculations with adjusted screening

Changing the screening necessitates an adjustment of the deformation potential V_D. So we repeated for Au the search for V_D following the procedure described earlier in this section. We found an increase of V_D from 4.6 to 5.8 eV.

This trick, however, is somewhat questionable, as the amount of extra screening by the *d* electrons will depend on the experimental conditions, in particular on the laser energy. Nevertheless we adopt the increase of the screening by 50% for all experiments. With these adjusted values of V_D and λ we repeated the calculations for Au. The results can be found in Figs. 6(b), 7, 8(a), and 8(b) and are indicated with SIM2. In fact the results are quite disappointing. First, the thermalization of the electron gas is too slow [Figs. 8(a) and 8(b)]. Furthermore, the temperature dependence of the relaxation time is now much too weak [Figs. 6(b) and 7]. We can understand this as follows. In the limit of the absence of *e-e* scattering the excited electrons can relax only by emission of phonons. As argued above under these circumstances the net emission is temperature independent, leading to a temperature-independent relaxation time. This effect is clearly visible when we decrease the strength of the *e-e* scattering (roughly speaking, the strength is proportional to $1/\lambda^4$, viz., about a factor of 4). So we are dealing with an inconsistent picture. The two different photoemission experiments require different strengths of the *e-e* interaction.

A solution to this dilemma may be the following. Shortly after the excitation we have holes in the *d* band. This may be a large number due to the high density of states. In such a situation the *d* band contributes to the screening. The holes are rapidly scattered into the *s* band and diffuse to the Fermi surface. The now completely filled *d* band does not contribute to the screening. So we start with a strong screening, which decreases gradually. The lifetime experiments investigate the first 100 fs, when the *e-e* interaction is relatively weak. On the other hand, the ''temperature'' and relaxation experiments deal with longer times, where the *e-e* scattering is stronger. In Ag the situation is different. We do not have excitations out off the *d* band and we can simply use the Thomas-Fermi screening of the *e-e* interaction.

F. Resistivity

The electron-phonon scattering is also responsible for the resistivity at higher temperatures. We calculated this resistivity in momentum relaxation-time approximation[28] using the value of V_D extracted from the analysis of the ultrafast experiments.

The results can be found in Figs. 10(a) and 10(b). For Ag the agreement between experiment[38] and calculation at 300 K is surprisingly good. For Au the predicted resistivity is 30% too low, but the agreement should still be considered as quite satisfactory. One has to keep in mind that V_D has been derived from a femtosecond transient reflectivity experiment analyzed by a Monte Carlo simulation in which approximations had to be made (see Sec. II). As mentioned above these approximations (the neglect of the *d* band) are more severe in the case of Au than in the case of Ag.

V. CONCLUSIONS

In the previous sections we have discussed in detail the analysis of experimental data on the energy relaxation and electron thermalization in Ag and Au using ensemble Monte Carlo simulations. In these calculations we started with only one free parameter, viz., the deformation potential in the electron-phonon coupling. We have obtained a consistent description for the available experimental data on Ag. It turned out that, we could have determined the deformation potential from the resistivity and the screening parameter from the high-energy lifetimes. These values give a good description of those experiments, where both interactions play a role.

For Au we had more experimental data at our disposal. If we apply the same procedure for Au as we did for Ag, we end up with an inconsistent picture, though a lot of the experimental data could be described quite well. The two different photoemission experiments, however, required a dif-

ferent strength of the electron-electron scattering as expressed by the screening parameter. It is undecided whether a two-band Monte Carlo simulation solves this problem. In such a calculation not only the e-ph scattering has to be updated (hot-phonon effects), but also a dynamical screening has to be incorporated. This item is not unimportant, since a simulation of magnetic-optical phenomena[19–21] requires the incorporation of the exchange-split d bands, which also will give time-dependent screening.

From this information we draw the important conclusion that we can use this technique for ultrafast processes in metals. This opens the possibility to apply the Monte Carlo method to other experimental data such as two-photon photoemission lifetime measurements or to thick films, where we can investigate the diffusion mechanism. In conclusion, the technique of Monte Carlo simulation has proven its value again and is a promising tool in the area of ultrafast processes in metals.

ACKNOWLEDGMENTS

The author wishes to thank his colleagues Wim de Jonge, Henk Swagten, Maarten van Kampen, Bart Smits, and Bert Koopmans for a critical reading of the manuscript. In particular, discussion with Bert Koopmans has been a great stimulus for this work. Illuminating discussions with Rogier Groeneveld, Rudolf Sprik, and Julius Hohlfeld also are gratefully acknowledged.

*Present address: Bos d'al Bas, 46230 Montdoumerc, France.

[1] See, e.g., Proceedings of the Conference on Hot Carriers in Semiconductors, HCIS-8, London, 1993 [Semi. Sci. Technol. **9** (1994)]; Proceedings of the Conference on Nonequilibrium Carrier Dynamics in Semiconductors, HCIS-10, Berlin, 1997 [Phys. Status Solidi B **204** (1997)].

[2] C. Jacoboni and L. Reggiani, Rev. Mod. Phys. **55**, 645 (1983).

[3] C. Jacoboni and P. Lugli, *The Monte Carlo Method for Semiconductor Device Simulation* (Springer, Vienna, 1989).

[4] C. Moglestue, *Monte Carlo Simulation of Semiconductor Devices* (Chapman and Hall, London, 1993).

[5] R. H. M. Groeneveld, R. Sprik, and A. Lagendijk, Phys. Rev. B **45**, 5079 (1992).

[6] T. Juhasz, H. E. Elsayed-Ali, X. H. Hu, and W. E. Bron, Phys. Rev. B **45**, 13 819 (1992).

[7] C. K. Sun, F. Vallee, L. H. Acioli, E. P. Ippen, and J. G. Fujimoto, Phys. Rev. B **50**, 15 337 (1994).

[8] T. Juhasz, H. E. Elsayed-Ali, G. O. Smith, C. Suarez, and W. E. Bron, Phys. Rev. B **48**, 15 488 (1993).

[9] C. Suarez, W. E. Bron, and T. Juhasz, Phys. Rev. Lett. **75**, 4536 (1995).

[10] J. Hohlfeld, J. G. Muller, S. S. Wellershoff, and E. Matthias, Appl. Phys. B: Lasers Opt. **64**, 387 (1997).

[11] W. S. Fann, R. Storz, H. W. K. Tom, and J. Bokor, Phys. Rev. Lett. **68**, 2834 (1992).

[12] W. S. Fann, R. Storz, H. W. K. Tom, and J. Bokor, Phys. Rev. B **46**, 13 592 (1992).

[13] C. A. Schuttenmaer, M. Aeschlimann, H. E. Elsayed-Ali, R. J. D. Miller, D. A. Mantell, J. Cao, and Y. Cao, Phys. Rev. B **50**, 8957 (1994).

[14] T. Hertel, E. Knoesel, M. Wolf, and G. Ertl, Phys. Rev. Lett. **76**, 535 (1996).

[15] S. Ogawa, H. Nagano, and H. Petek, Phys. Rev. B **55**, 10 869 (1997).

[16] J. Cao, Y. Gao, R. J. D. Miller, H. E. Elsayed-Ali, and D. A. Mantell, Phys. Rev. B **56**, 1099 (1997).

[17] M. Wolff and M. Aesclimann, Phys. Blatter **54**, 145 (1998).

[18] J. Cao, Y. Gao, H. E. Elsayed-Ali, R. J. D. Miller, and D. A. Mantell, Phys. Rev. B **58**, 10 948 (1998).

[19] E. Beaurepaire, J. C. Merle, A. Daunois, and J. Y. Bigot, Phys. Rev. Lett. **76**, 4250 (1996).

[20] J. Hohlfeld, E. Matthias, R. Knorren, and K. H. Bennemann, Phys. Rev. Lett. **78**, 4861 (1997).

[21] M. Aeschlimann, M. Bauer, S. Pawlik, W. Weber, R. Burgermeister, D. Oberli, and H. C. Siegmann, Phys. Rev. Lett. **79**, 5158 (1997).

[22] B. Koopmans, M. van Kampen, J. T. Kohlepp, and W. J. M. de Jonge, Phys. Rev. Lett **85**, 844 (2000).

[23] M. I. Kaganov, I. M. Lifshitz, and L. V. Tanatarov, Zh. Eksp. Teor. Fiz. **31**, 732 (1957) [Sov. Phys. JETP **4**, 173 (1957)].

[24] R. Groeneveld, R. Sprik, and A. Lagendijk, Phys. Rev. B **51**, 11 433 (1995).

[25] D. Bejan and G. Raseev, Phys. Rev. B **55**, 4250 (1997).

[26] R. Knorren, K. H. Bennemann, R. Burgermeister, and M. Aeschlimann, Phys. Rev. B **61**, 9427 (2000).

[27] N. W. Ashcroft and N. D. Mermin, *Solid State Physics* (Holt-Saunders, Philadelphia, 1976).

[28] O. Madelung, *Introduction to Solid State Theory* (Springer, Berlin, 1981).

[29] P. H. Dederichs, H. Schober, and D. J. Sellmyer, *Phenon States. Electron States and Fermi Surfaces of Alloys*, edited by K.-H. Hellwege and J. L. Olsen, Landolt-Börnstein, Tables Group III, Vol. 13, Pt. a (Springer, Berlin, 1982).

[30] P. Kocevar, Physica B & C **134B+C**, 155 (1985).

[31] C. J. Hearns, in *The Physics of Nonlinear Transport in Semiconductors*, edited by D. K. Ferry *et al.* (Plenum, New York, 1980).

[32] P. J. van Hall and P. M. W. Blom, Superlattices Microstruct. **13**, 329 (1993).

[33] D. Pines and P. Nozieres, *The Theory of Quantum Liquids* (Benjamin, New York, 1966), Vol. I.

[34] J. J. Quin and R. A. Ferrel, Phys. Rev. **112**, 812 (1958).

[35] R. Rosei, Phys. Rev. B **10**, 474 (1974).

[36] R. Groeneveld, thesis, University of Amsterdam, 1992.

[37] T. Kuhn and F. Rossi, Phys. Rev. B **46**, 7496 (1992).

[38] J. Bass and K. H. Fischer, *Metals: Electronic Transport Phenomena*, edited by K.-H. Hellwege and J. L. Olsen, Landolt-Börnstein, Tables, Group III, Vol. 15, Pt. a (Springer, Berlin, 1981).